Applied Catalysis B: Environmental 250 (2019) 132–142

Contents lists available at ScienceDirect

Applied Catalysis B: Environmental

journal homepage: www.elsevier.com/locate/apcatb

A robust core-shell silver soot oxidation catalyst driven by Co_3O_4: Effect of tandem oxygen delivery and Co_3O_4-CeO_2 synergy

Xin Wang[a,1], Baofang Jin[b,1], Ruixue Feng[a], Wei Liu[a], Duan Weng[b], Xiaodong Wu[b,*], Shuang Liu[a,*]

[a] School of Materials Science and Engineering, Ocean University of China, Qingdao 266100, China
[b] Key Laboratory of Advanced Materials of Ministry of Education of China, School of Materials Science and Engineering, Tsinghua University, Beijing 100084, China

ARTICLE INFO

Keywords:
Co_3O_4
Ag/CeO_2
Soot oxidation
NO oxidation
Tandem oxygen delivery

ABSTRACT

In this work, tandem oxygen delivery systems were built by coating cube-like Co_3O_4 with Ag/CeO_2, which exhibited high soot oxidation activity that overwhelmed the Fe_2O_3-based catalysts. The results of TPR and activity tests indicated that a large amount of Co_3O_4 lattice oxygen could be transferred into O_x^- with the assistance of Ag/CeO_2. These active oxygen species accelerated the oxidation of soot and NO at low temperature. Furthermore, the Co_3O_4-CeO_2 synergy facilitated $Co^{3+} \rightarrow Co^{2+}$ transformation during reactions, resulting in boosted NO conversion and thereby NO_2-assisted soot combustion at mild and high temperatures. Given the $Ag/Co_3O_4@CeO_2$-type catalysts were low-cost, hydrothermally stable and could be fabricated via co-precipitation methods easily, they were highly promising for application in both gasoline and diesel particulate filters.

1. Introduction

Soot, an unwelcome byproduct of mobile engines is commercially eliminated via trap-and-burn technology, i.e. diesel/gasoline particulate filters (DPF/GPFs) [1,2]. In order to regenerate the sooted DPFs mildly, catalyzed filters loaded with platinum (CDPFs) were developed, which could oxidize soot efficiently with the assistance of strong oxidizing NO_2 [3,4]. However, platinum is expensive and ineffective for soot combustion in absence of NO_x (a typical working condition of CGPFs) [5,6], low-cost substitutes with broader applicability are thereby in demand.

With gaseous O_2 as the oxidant, the key active species for soot combustion are "active oxygen" (O_x^-). According to Haber [7,8], these electrophilic reactants may attack the π-bond system of aromatics and cause deep oxidation. Among all catalysts, Ag/CeO_2 was proven one of the best O_x^- providers, which was able to convert both O_2 and CeO_2 lattice oxygen into O_x^- rapidly [9–11]. Consequently, Ag/CeO_2 exhibited high soot oxidation activity under simulated GPF environment (no NO_x, low O_2 concentration) [12,13]. Furthermore, we recently observed that by grafting Ag/CeO_2 polycrystals (the "shell") on the surface of Fe_2O_3 (the "core"), the bulk oxygen inside Fe_2O_3 could be fully utilized to yield O_x^-, resulting in fast and stable soot combustion with only little gaseous O_2 (1%) involved [14]. However, it is noted that there will be no oxygen inlet for GPFs if the upstream TWC works under stoichiometric conditions [15]. This means that, excess O_2 is available for the catalysts only through or during fuel cut coast-down conditions, in which situation the inlet temperature of CGPFs will decrease obviously [16]. Therefore, catalysts like $Ag/Fe_2O_3@CeO_2$ which can hardly eliminate soot at temperature below 300 °C may not be practical enough. What is worse, Fe_2O_3 is a poor NO oxidizer (e.g. maximum $NO \rightarrow NO_2$ conversion < 30% [17]), which cannot make full use of NO_x to combust soot (the "NO_2-assited" mechanism) [18,19] and thereby shows low practical potential for CDPFs [6]. In this sense, replacing Fe_2O_3 with more robust oxides is a good way for the sake of practicality.

Co_3O_4 can be such a choice. On one hand, with lower effective activation energy, Co_3O_4 loses its lattice oxygen much easier than Fe_2O_3 does [20], making the former a more effective igniter. For example, Co_3O_4 has been long proven the most reactive transition metal oxide for catalytic combustion of soot [21], CO [22], ammonia [23], methane [24] and many other hydrocarbons [7,8]. On the other hand, Co_3O_4 shows high $NO \rightarrow NO_2$ conversion (higher turnover rate than platinum, maximum conversion > 65%) [25–27], which can be further improved after CeO_2 loading [28]. In sum, Co_3O_4-CeO_2 mixed oxides can oxidize soot through both the "O_2-assisted" (using O_x^- as a direct active phase) and the "NO_2-assisted" (using NO_2 as an indirect active phase) routes [19], making them promising catalysts for both gasoline and diesel soot removal [29,30]. To maximize the catalytic performance, it is worth

* Corresponding authors.
E-mail addresses: wuxiaodong@tsinghua.edu.cn (X. Wu), lius@ouc.edu.cn (S. Liu).
[1] These two authors contributed equally to this work.

https://doi.org/10.1016/j.apcatb.2019.03.019
Received 7 December 2018; Received in revised form 11 February 2019; Accepted 7 March 2019
Available online 07 March 2019
0926-3373/

trying to build $Ag/Co_3O_4@CeO_2$ catalysts with a tandem oxygen delivery route ($Co_3O_4 \rightarrow CeO_2 \rightarrow Ag$) [14]. In addition, the Co_3O_4 core should be consisted of nanocube-like Co_3O_4 monocrystals. This is because, the nanocubic Co_3O_4 not only selectively exposes the {100} facets that highly reactive for some (e.g. CO and soot) oxidation reactions [31,32], but also is small enough (i.e. < 50 nm in size [24,33], like the nanocubic Fe_2O_3 in ref. [14]) to enlarge the Co_3O_4-CeO_2 interface area and thereby boost the oxygen delivery.

It is worth noting that, although Co_3O_4-CeO_2 was an old recipe for soot oxidation catalysts [34], several questions in terms of its reaction mechanism remained unsolved. First, the catalytic effectiveness of large Co_3O_4 particles (e.g. > 20 nm in size) is in ambiguous. In the past, highly dispersed Co^{3+} species were recognized as indispensable active phases, while their aggregation caused negative impacts [35–38]. Contrarily, according to Iglesia et al. [25], the intrinsic NO oxidation activity increased with increasing Co_3O_4 cluster size, indicating large Co_3O_4 grains may be promising NO_x-assisted soot oxidizers. Second, ever since the outstanding soot oxidation activity of Co_3O_4-CeO_2 (in comparison with Co_3O_4-Al_2O_3, Co_3O_4-SiO_2 and Co_3O_4-SnO_2) was recognized by Harrison et al. at 2003 [34], this unique $Co_3O_4 \leftrightarrow CeO_2$ synergy was repeatedly reported to be essential for NO and soot oxidation [36–38]. These results, however, did not coincide with the fact that Co_3O_4-SiO_2 and even unsupported Co_3O_4 particles are also highly active NO oxidizers [25–27]. In this sense, the specific roles of Co_3O_4, CeO_2 and their interaction in the reactions deserve to be re-evaluated. Finally, the introduction of silver brought in additional complexity. For example, though NO_2 was proven an excellent soot igniter [19], there were reports indicated that silver-based catalysts (e.g. Ag/Co_3O_4-CeO_2 and Ag/Al_2O_3) exhibited worse soot oxidation after involving NO_x [30,39]. All the above inconsistencies called for further investigation over the Ag/Co_3O_4-CeO_2 system.

In this study, core-shell catalysts with tandem oxygen delivery routes ($Ag/Co_3O_4@CeO_2$) were built based on highly reactive Co_3O_4 nanocubes. As expected, these catalysts oxidized soot efficiently under both the simulated DPF and GPF environment, whose structure-activity relationship was further explored detailedly based on various characterizations.

2. Experimental section

2.1. Catalyst synthesis

$AgNO_3$, $Ce(NO_3)_3{\cdot}6H_2O$, $Co(NO_3)_2{\cdot}6H_2O$, $CoCl_2{\cdot}6H_2O$, ethanol, $Fe(NO)_3{\cdot}9H_2O$, hexamethylenetetramine (HMT), $KClO_3$, KOH, *N,N*-dimethylformamide (DMF), polyvinylpyrrolidone (PVP, Mw = 58,000) and $Pt(NO_3)_2$ solution (18.02%) were purchased from Aladdin. All the chemicals were used as received without further purification.

Both the nanocube-like Co_3O_4 (denoted as "**Co**") and Fe_2O_3 (denoted as "**Fe**") were obtained through hydrothermal methods [14,33]. For the synthesis of **Co**, an aqueous KOH (1.12 g) + $KClO_3$ (0.613 g) solution (20 ml) was added dropwise into an aqueous solution (30 ml) dissolving 2.38 g of $CoCl_2{\cdot}6H_2O$ and 5.55 g of PVP. The mixture was stirred for 30 min, transferred into a Teflon-lined stainless-steel autoclave (100 ml) and heated at 120 °C for 20 h. For the synthesis of **Fe**, 0.289 g of $Fe(NO_3)_3{\cdot}9H_2O$ and 0.628 g of PVP were dissolved in 25.7 ml of DMF, which was kept at 180 °C for 30 h in a Teflon-lined stainless steel autoclave (50 ml). Both the Co_3O_4 and Fe_2O_3 products were collected by centrifugation at 8500 rpm for 30 min, followed by washing at least 3 times with water and ethanol.

CeO_2 grafting was achieved by a chemical precipitation method [14]. Typically, 0.05 g of **Co** or **Fe** powders were dispersed in a water-ethanol (50%-50%) mixture (40 ml). After ultrasonic treatment for 15 min, certain amounts of $Ce(NO_3)_3{\cdot}6H_2O$ (0.081 g for **Co** and 1.3 g for **Fe**) and HMT (keeping the pH at 7.35) were added. This suspension was heated to 70 °C in flowing N_2 and maintained at this temperature under reflux and vigorous stirring for 2 h. The products were collected by centrifugation, washed and dried at 110 °C. Finally, **Co@Ce** and **Fe@Ce** catalysts were obtained after calcinations at 500 °C in static air for 2 h. The Ag (5 wt.%) containing catalysts (**Ag/Co@Ce** and **Ag/Fe@Ce**) were prepared by incipient wetness impregnation of the above **Co@Ce** or **Fe@Ce** with aqueous $AgNO_3$ solution. Each impregnation process was followed by drying (110 °C) and calcinations (500 °C).

In order to make comprehensive comparison, CeO_2 (denoted as "**Ce**") and Co_3O_4-CeO_2 (denoted as "**CoCe**") catalysts were prepared via precipitation methods. Generally, KOH solution was added dropwise into an aqueous solution (100 ml) dissolving certain amount of Ce $(NO_3)_3$ and $Co(NO_3)_2$. As soon as the pH came up to 9, the precipitate was allowed to settle for 4 h, collected by filtration and washed. After calcinations at 500 °C for 2 h, **Ce** and **CoCe** samples were thus obtained. Notably, **CoCe** and **Co@Ce** shared the identical Co:Ce atomic ratio (5:1, measured by ICP-AES using an Agilent 725). In addition, **Ag/CoCe** (silver content: 5 wt.%) was obtained by impregnating aqueous $AgNO_3$ solution on **CoCe** and calcinations.

To evaluate the catalysts' practicality, platinum catalysts (Pt/Al_2O_3 with platinum content of 1 wt.%) were synthesized via incipient wetness impregnation. Detailed processes can be found in ref. [13]. The platinum catalysts were pre-reduced in H_2 before catalytic tests.

2.2. General characterizations

The solid properties of the catalysts were explored with a X–ray diffractometer (D8 ADVANCE, Bruker, Germany), a transmission electron microscopy (JEOL 2100, JEOL Ltd., Japan) with a point resolution of 0.19 nm and N_2 adsorption/desorption isotherms at −196 °C (JW–BK122 F, Beijing JWGB, China). Chemical states of the catalysts were measured by X–ray photoelectron spectra (ESCALAB 250 Xi, ThermoFisher Scientific, USA) with a monochromatic Al K_α (1486.6 eV) X–ray source. Raman spectra were obtained through a LabRAM HR 800 (HORIBA Jobin Yvon, France) with a detective laser of 532 nm.

2.3. Specific characterizations

The catalysts' reducibility was evaluated by hydrogen temperature-programmed reduction (H_2-TPR, -20 °C~450 °C) tests, in which a Micromeritics AutoChem II 2920 was used to monitor the H_2 consumption as TCD signals.

In order to detect the dynamic change (generation → consumption → generation…) of ceria surface oxygen, cycled TPR tests were performed according to the procedure shown in Scheme 1. At the beginning of the tests, the catalyst (50 mg) was pre-oxidized in 1% O_2/He (50 ml/min) at 300 °C for 10 min. After being cooled down to -20 °C, flushed by He for 10 min, it experienced a H_2-TPR test (denoted as "O_2-1st"). The second H_2-TPR test (O_2-2nd) was performed subsequently after a similar pre-oxidation process. Both TPR tests were terminated at 350 °C. At this temperate, all the ceria surface oxygen could be consumed without changing catalysts' structural properties [11,12].

2.4. Soot oxidation activity measurements

Printex–U (Degussa) was used as the model soot. For each test, the "tight" (grinding in an agate mortar for 5 min) or "loose" (mixing with a spatula for 2 min) catalyst (100 mg) & soot (10 mg) mixtures were diluted with SiO_2 pellets (300 mg), sandwiched by quartz wool and then placed in a vertical fixed–bed quartz reactor. A gas mixture of 1% O_2/N_2 (500 ml/min, GHSV = 100,000 h^{-1}) was used to mimic the CGPF working conditions. It is worth noting that, without extra air injection downstream the TWC, a continuous stream of 1% O_2 cannot be maintained inside a real GPF [15]. Therefore, this widely accepted reaction condition [40–42] can only be regarded as quantitative simulation of the oxygen-lacking environment of the catalysts in CGPF. Meanwhile, a gas flow containing 500 ppm NO and 5% O_2 balanced by N_2 (500 ml/min, GHSV = 100,000 h^{-1}) was applied to simulate the CDPF working

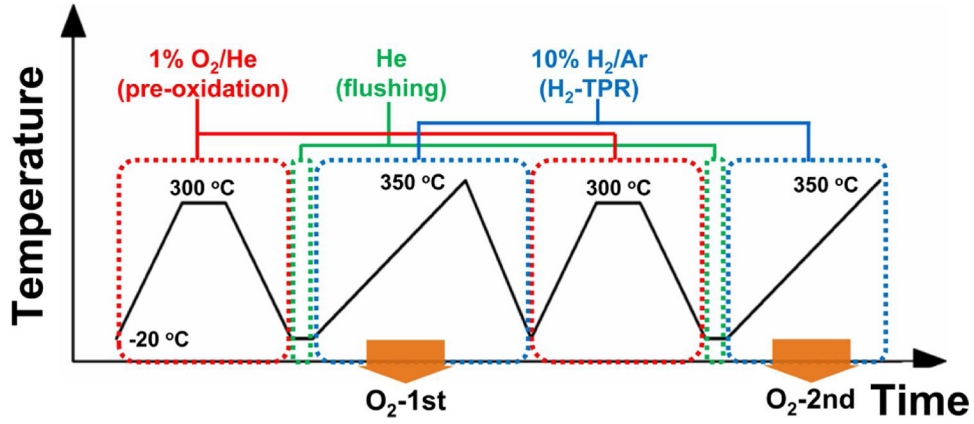

Scheme 1. Scheme of the experimental procedure for cycled H_2-TPR tests.

conditions. The influence of H_2O was measured by adding 5% water vapor into each atmosphere.

The catalytic oxidation of soot was mainly performed in a temperate-programmed way (soot-TPO, 5 °C/min) with downstream gases monitored by an infrared spectrometer (Thermo Nicolet iS10). Specifically, for reactions in 1% O_2/N_2 and "tight" contact, extra isothermal reactions were performed at relatively temperatures and thereby low soot conversions (< 10%).

2.5. NO oxidation activity measurements

NO temperature-programmed oxidation (NO-TPO) tests were performed in the same apparatus that used in soot-TPO. In a typical test, catalysts (100 mg) diluted by SiO_2 pellets (300 mg) were heated from room temperature to 600 °C (5 °C/min) in 500 ppm NO/5% O_2/N_2 (500 ml/min). Additionally, isothermal NO oxidation tests were performed at 220 °C to fully evaluate the catalysts' NO oxidation performance. During the isothermal reaction, the inlet atmosphere (500 ml/min) was switched from 500 ppm NO/5% O_2/N_2 to 500 ppm NO/N_2 (denoted as "O_2 cut off").

3. Results

3.1. Solid properties

The XRD patterns of the catalysts are shown in Fig. 1. Clearly, Fe and Co exhibited typical phases of α-Fe_2O_3 and Co_3O_4 with high crystallinity, respectively [14]. After CeO_2 coating, the cubic fluorite phase of ceria was observed over both Fe@Ce and Co@Ce. The crystallinities obtained by using Scherrer equation (Table 1) suggested that the polycrystalline ceria was consisted of small CeO_2 grains (5.5˜6.5 nm in size). Co@Ce and the stantard ceria shared a similar CeO_2 lattice constant (0.5411 nm), which was different from that of Fe@Ce (0.5397 nm). This implied that the interfacial ceria-based solid solutions formed in Fe@Ce but not in Co@Ce [14]. Moreover, besides the unconspicuous Ag° diffraction peaks at 2θ = 38.2° and 44.3°, silver loading caused little change in the catalysts' structure. No trace of Ag_xO, $FeCeO_x$, $CoCeO_x$ were detected on any of the samples.

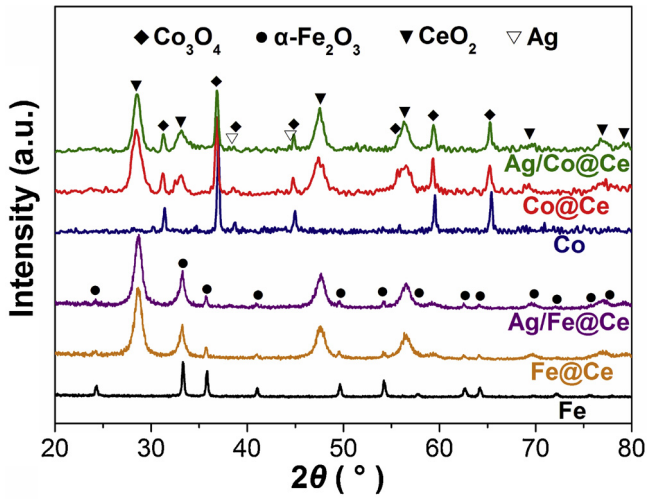

Fig. 1. XRD patterns of the catalysts.

The morphologies of the catalysts are shown in Fig. 2. Both Fe and Co were consisted of uniform cube-like monocrystals selectively exposing their {012} and {100} facets, respectively [14,33]. The Co_3O_4 cubes were smaller than the Fe_2O_3 ones (36 nm v.s. 45 nm). Both Fe@Ce and Co@Ce were covered with polycrystalline CeO_2 layers (6˜10 nm thick). These loosely arranged CeO_2 grains conferred interval for gas exchanging with the inner cores, resulting in higher external surface areas of Fe@Ce and Co@Ce than Fe_2O_3 and Co_3O_4, respectively (Table 1). Impregnation of silver onto the CeO_2 layers gave rise to well dispersed Ag nanoparticles (1.5–3 nm). No AgO_x was observed. Since the crystallite size data obtained from XRD and TEM agreed well with each other (Table 1), it was suggested that the designed Ag/Co_3O_4@CeO_2 core-shell structure was built successfully.

3.2. Chemical states

Information about the chemical states of surface elements was obtained by XPS. As shown in Fig. 3a and Table 1, there was less Ce^{3+} on Co@Ce than on Fe@Ce, which was almost unaltered after silver loading. Notably, the Ce^{3+}/Ce^{4+} value of Ag/Co@Ce (0.27) was significantly lower than that of traditional polycrystalline Ag/CeO_2 samples (0.37˜0.52) [13]. Similar phenomenon was observed over Fe_2O_3@CeO_2 earlier and ascribed to the Fe_2O_3 → CeO_2 oxygen transfer during catalyst synthesis [14,43]. Given the effective activation energy of Co_3O_4 is lower than Fe_2O_3 [20], such oxygen transfer may work more easily at the Co_3O_4-CeO_2 interface, resulting in lattice oxygen enrichment in the as-received CeO_2 grains around Co_3O_4.

Different from Ce, the quantification of Co^{3+} and Co^{2+} was not straightforward due to their close binding energy [32]. Based on the results of Biesinger and Kang et al. [44,45], the intense satellite peaks of Co^{2+} (785–792 eV and 800–808 eV) made it distinguishable from Co^{3+}. Clearly, all the samples in Fig. 3b exhibited typical Co 2p spectra of Co_3O_4 [44], while the content of Co^{2+} decreased after CeO_2 coating. This should be attributed to the buffer-like Co_3O_4-CeO_2 interaction, which was caused by redox equilibrium (Ce^{4+}/Ce^{3+} ↔ Co^{3+}/Co^{2+}) and observed widely over CoO_x-CeO_2 and CuO_x-CeO_2 systems [29,45–47]. During catalyst synthesis (e.g. calcinations at 500 °C in air),

Table 1
Summary of structural data of the catalysts.

Catalyst	S_{Ext} (m^2/g)[a]	CeO_2 crystallite size (nm)[b]	Lattice constant of CeO_2 (nm)	Surface Ce^{3+}/Ce^{4+}[c]	Co_3O_4 or Fe_2O_3 crystallite size (nm)[b]	Ag crystallite size (nm)[b]
Co	31.7	–	–	–	37.0	–
Co@Ce	38.5	5.7	0.5411	0.27	34.5	–
Ag/Co@Ce	37.1	6.0	0.5410	0.27	35.7	< 3
Fe	25.7	–	–	–	43.3	–
Fe@Ce	29.4	6.2	0.5397	0.38	46.1	–
Ag/Fe@Ce	27.1	6.4	0.5395	0.38	43.4	< 3

[a] External surface area obtained from N_2 physisorption tests at −196 °C.
[b] Obtained from both the TEM and XRD (Scherrer equation) data.
[c] Obtained from the XPS data.

once Co_3O_4 delivered its lattice oxygen to CeO_2, the as-formed oxygen vacancies (V_O) were refilled by gaseous O_2 through the interval of CeO_2 grains. This re-oxidation process went faster than the formation of V_O [48] and was further accelerated by the presence of ceria [47]. As a result, both CeO_2 and Co_3O_4 in the as-received Co@Ce and Ag/Co@Ce catalysts were enriched with lattice oxygen. In addition, as shown in Fig. 3b, the catalytic oxidation of both soot and NO led to slight increase in the Co^{2+} content of Co@Ce, indicating the reduction of cobalt during these reactions.

For both Ag/Co@Ce and Ag/Fe@Ce, the silver species exhibited Ag $3d_{5/2}$ binding energies at ~368.1 eV and a splitting of 6 eV (Fig. 3c), indicating they existed in the form of metallic Ag°. This was in accordance with the results in XRD and TEM, which was attributed to the accelerated decomposition of AgO_x and Ag^+-Ce^{3+} electron transfer during catalyst synthesis [12].

3.3. Active species on the catalysts

The surface electrophilic O_x^- species were proven important active phases for soot catalytic combustion [9–13]. Raman spectroscopy and H_2-TPR were applied to make their qualitative and quantitative analysis, respectively. As shown in Fig. 4a, Co@Ce exhibited more intensive Raman bands at 800~980 cm^{-1} than Fe@Ce, indicating there was more peroxide (O_2^{2-} or O^-) on the former sample [49]. Silver loading gave remarkable rise to both O^- (825~883 & 951~964 cm^{-1}) and O_2^- (1158~1126 cm^{-1}) species on Ag/Co@Ce and Ag/Fe@Ce, which could be rationalized along two lines. On one hand, metals with low work function (like silver) may induce long-range charge transfer (metal → CeO_2) and thereby induce oxygen back spillover under the electric field (the Cabrera–Mott theory) [13,50]. The "pumped out" ceria lattice oxygen could then transfer into O_x^- through surface equilibria ($O^{2-} \leftrightarrow O^- \leftrightarrow O_2^- \leftrightarrow O$) [7,8]. On the other hand, as a traditional epoxidation catalyst, silver could chemisorb and activate gaseous O_2 through $Ag + O_2 \rightarrow Ag^+ + O_2^-$ [12,51]. Thanks to the oxygen from both ceria lattice and gaseous O_2, there came out to be more O_x^- on Ag/Co@Ce and Ag/Fe@Ce than on the silver-free catalysts [11,14].

Quantitative information about active species was obtained by the H_2-TPR tests. As shown in Fig. 4b, hydrogen could reduce both Co_3O_4 ($Co_3O_4 \rightarrow CoO \rightarrow Co$) [31,32] and Fe_2O_3 ($Fe_2O_3 \rightarrow Fe_3O_4$) [14] at temperatures below 350 °C. However, due to the weaker reducing ability of soot/NO in comparison with H_2, both Co and Fe remained stable during the soot/NO oxidation tests (Fig. 3b and Figure S1) [14]. Therefore, it was meaningless to correlate the catalysts' activities with the reduction of Co_3O_4 or Fe_2O_3. Instead, the low-temperature H_2 consumption caused by O_x^- was an appropriate reactivity descriptor [13]. As indicated by Fig. 4c, the amounts of O_x^- species on Co and Fe were low, while each modification (i.e. CeO_2 coating and silver loading) resulted in drastic enhancement of O_x^-. Specifically, Ag/Co@Ce exhibited the largest content of O_2^- among the samples, which agreed well with the Raman data. In addition, given there was no AgO_x on the as-received catalysts (Fig. 3c), the contribution of AgO_x to H_2 consumption was not considered.

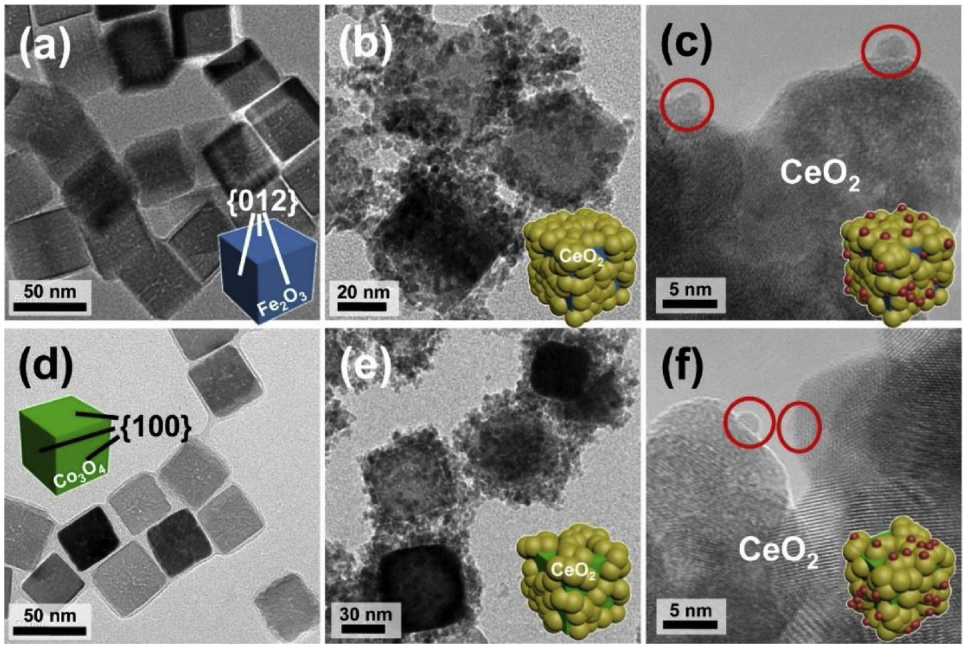

Fig. 2. Typical HRTEM images of (a) Fe, (b) Fe@Ce (c) Ag/Fe@Ce-F, (d) Co, (e) Co@Ce and (f) Ag/Co@Ce. Silver nano-particles were marked with red circles. Fe_2O_3, Co_3O_4, CeO_2 and Ag were represented by blue, green, yellow and red polyhedrons in the schematic models, respectively (For interpretation of the references to colour in this figure legend, the reader is referred to the web version of this article).

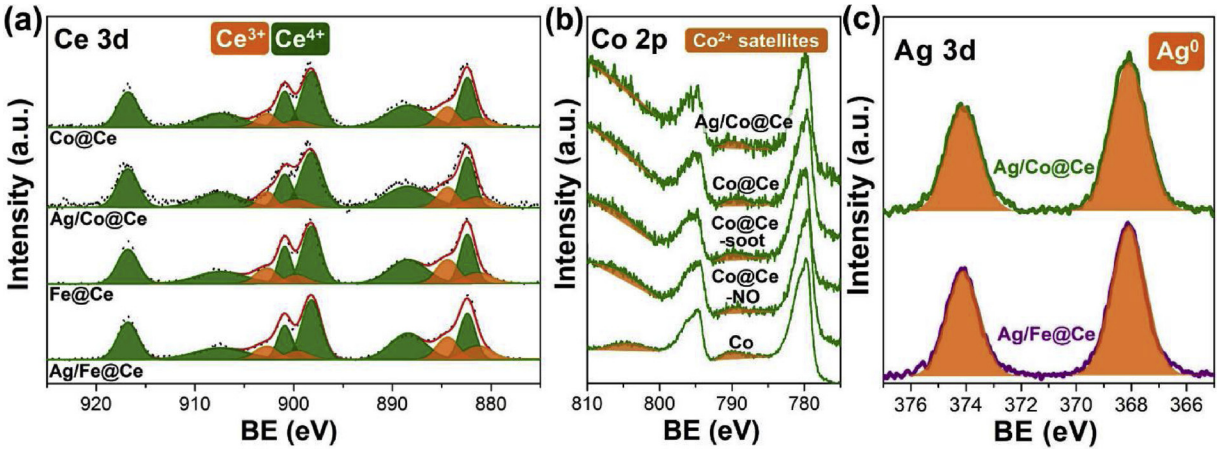

Fig. 3. XPS spectra of the catalysts in (a) Ce 3d, (b) Co 2p and (c) Ag 3d core level regions. Co@Ce-soot, Co@Ce-NO and Co-NO refer to catalysts that experienced isothermal soot oxidation (1% O_2, tight contact) or NO oxidation (500 ppm NO/5% O_2/N_2) tests at 225 °C for 30 min.

3.4. Consumption and regeneration of active species

The Raman and H_2-TPR results demonstrated that Co, Co@Ce and Ag/Co@Ce exhibited progressively higher O_x^- generation ability. Since NO/soot oxidation proceeds through Mars-van Krevelen cycles on reducible metal oxides [13], the regeneration of consumed active species can be as important as their initial presence. As shown in Fig. 5a and Table 2, after being reduced by H_2 and re-oxidized by O_2 at 300 °C, Co_3O_4 consumed 14% less H_2 in the O_2-2nd test than in O_2-1st. This demonstrated that Co_3O_4 itself regained only partial of its initial lattice oxygen after one given reduction-oxidation cycle. In contrast, the cobalt species in Ag/Co@Ce were not only fully regenerated after one redox cycle (Table 2), but also became more reducible. As demonstrated by the O_2-2nd data in Fig. 5c, the Co_3O_4-drived H_2 consumption of Ag/Co@Ce completed at temperatures < 250 °C, at which the Co catalyst just started to consume H_2 (Fig. 5a). These results indicated that the ceria-based outer layers could amplify the reducibility of Co_3O_4, which was in accordance with the results of XPS (Fig. 3b) and earlier studies [28,29,45,46].

The amount of surface O_x^{n-} (x = 1 or 2) was quantified by the low-temperature H_2 consumption of Co@Ce and Ag/Co@Ce [13]. As shown in Fig. 5b, the oxidation pretreatment of Co@Ce gave rise to extra electrophilic O_x- (the O_2-1st data) that got regenerated easily once consumed (the O_2-2nd data in Table 2). Meanwhile, cobalt species in Co@Ce consumed H_2 at similar temperatures (> 150 °C) during the O_2-1st and O_2-2nd tests. In this sense, Co@Ce exhibited high redox stability. The presence of silver further increased the amount of O_x^{n-}. Interestingly, after reduction and re-oxidation with gaseous O_2 at 300 °C, 182% O_x^{n-} species got regenerated on Ag/Co@Ce (the O_2-2nd data in Table 2). This superior oxygen regeneration ability could accelerate the Mars-van Krevelen cycle of Ag/Co@Ce.

3.5. Activity of catalysts in O_2

Generally, catalysts' performance for Mars-van Krevelen-like reactions (e.g. soot ignition) depends crucially on their redox ability, especially when little gaseous O_2 is involved [8]. This point was reconfirmed by the soot-TPO results shown in Fig. 6a,b and Table 3. In a simulated CGPF working condition (1% O_2/N_2), lattice oxygen from the highly reducible Ag/Co@Ce filled the demand for "active oxygen" well, resulting in its low soot ignition temperature. Under both the "tight" and "loose" contact modes, the T_{50} (temperature at which 50% soot was

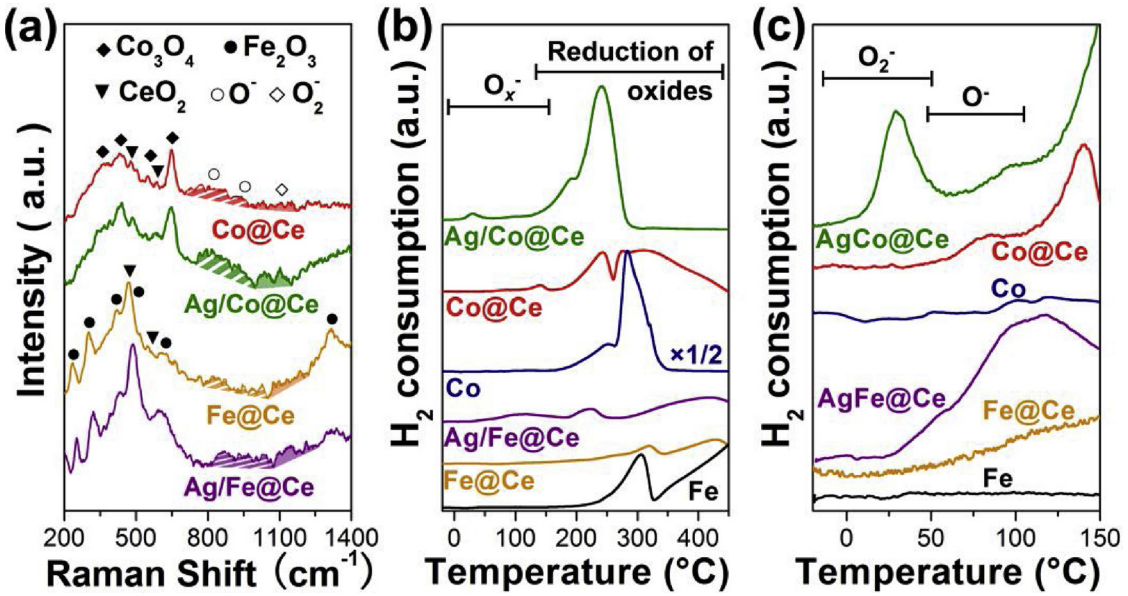

Fig. 4. (a) Visible Raman spectra, (b) H_2-TPR curves and (c) enlarged low-temperature H_2-TPR results. The shadowed and filled areas indicate the presence of O^- and O_2^-, respectively.

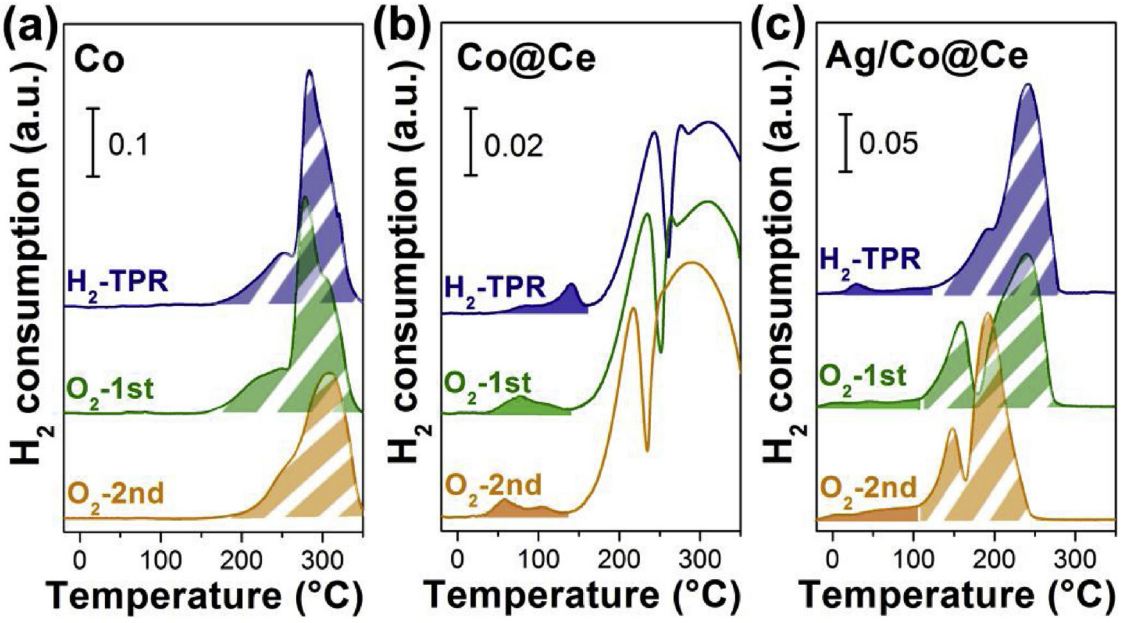

Fig. 5. Cycled H_2-TPR results of the Co_3O_4-based catalysts. The shadowed and filled areas refer to H_2 consumed by Co_3O_4 and O_x^{n-} on CeO_2 surface, respectively.

converted into CO_x) of Ag/Co@Ce was at least 30 °C lower than that of any other catalysts. Besides, Ag/Fe@Ce and Co@Ce with more O_x^- (Fig. 4) and faster active oxygen supply rate [14] exhibited obviously higher soot oxidation activity than Fe@Ce. All the catalysts exhibited high selectivity to CO_2 ($CO_2/CO_x > 99\%$) during the tests. Notably, Co_3O_4 and Fe_2O_3 were worse soot oxidizers than mixed oxides [14,28,38], while they were also inaccessible for soot particles (> 25 nm) after being coated by CeO_2. Therefore, the soot oxidation activities of Co and Fe themselves were not explored directly in this study.

Previously, it was evidenced that the activity of ceria-based catalysts for soot-TPO was actually appearance of the catalysts' activation and/or deactivation behavior during the reactions [11,12]. Therefore, it was important to evaluate the time-on-stream soot oxidation behavior of catalysts. As shown in Fig. 6c-1, by setting the reaction temperature at 200 °C, Co@Ce lost 66% of its initial activity after time-on-stream reaction for 800 s. In contrast, Ag/Co@Ce was not only twice active but also more stable than Co@Ce. Given the deactivation of ceria-based soot oxidation catalysts came mainly from insufficient O_x^- (especially O_2^-) supplement [11], the reaction stability of Ag/Co@Ce should be attributed to its high redox stability (Table 2). Being initially more active and catalytically stable, Ag/Co@Ce ignited soot at lower temperature in comparison with Co@Ce (Fig. 6a). At 225 °C, Co@Ce was warm enough to produce O_x^- rapidly and thereby became stable during the reactions (Fig. 6c-2). Fe@Ce got activated at ≥ 250 °C, with activity 15 times lower than that of Co@Ce (Fig. 6c-3).

It is worth noting that, in comparison with the easily deactivated Ag/CeO_2 catalysts reported earlier [12,13], Ag/Co@Ce and Ag/Fe@Ce were both catalytically stable during isothermal soot oxidation tests. This reconfirmed the effectiveness of using tandem oxygen delivery routes ($MO_x \rightarrow CeO_2 \rightarrow Ag$) to provide active species for soot combustion, especially when the regeneration of lattice oxygen from gaseous oxygen was rate-determining (e.g. under 1% O_2) [14].

3.6. Activity of catalysts in NO + O_2

As mentioned before, catalysts in CDPFs may act as NO oxidizers to combust non-contact soot particles with the assistance of gaseous NO_2 [19]. Under a simulated CDPF condition (500 ppm NO/5% O_2/N_2), the combustion of loosely contacted soot went more easily over Ag/Co@Ce and Co@Ce than over the Fe_2O_3-based catalysts (Fig. 7a and Table 3). This could be attributed to the superior NO oxidation activity of the Co_3O_4 inner cores [25–28], which were accessible for NO even after being coated by CeO_2. As shown in Fig. 7b, Co_3O_4 oxidized NO much more efficiently (65% maximal conversion at 280 °C) than Fe_2O_3 (21% maximal conversion at 360 °C) did. Interestingly, the loading of the least reactive CeO_2 (20% maximal conversion at 380 °C) and relatively inactive Ag [39] improved the activity of both Co_3O_4 and Fe_2O_3 obviously. In any case, the Co_3O_4-based samples were far better NO oxidizers than the Fe_2O_3 ones. The strong oxidizing NO_2 ignited soot at low temperatures and generated surface oxygen complexes (SOCs) that could be further decomposed into CO_x [4,52]. Consequently, Ag/Co@Ce with the highest NO_2 production (83% maximal conversion at 255 °C) combusted 10% soot at temperature as low as 298 °C.

To gain insight into the promotion effects of silver and ceria on NO oxidation, the reaction was performed isothermally at 220 °C with a cut-off of gaseous oxygen supply. As shown in Fig. 7c, the steady-state activity of catalysts followed a sequence identical to that in NO-TPO: Ag/Co@Ce > Co@Ce > Co. Interestingly, Co_3O_4 was deactivated drastically once the supply of O_2 was cut off, while the activity of Co@Ce and Ag/Co@Ce decreased much slowly. After reacting with NO anaerobically for minutes, all the catalysts tended to exhibit quasi-

Table 2
Quantitative analyses of H_2 consumption during the cycled H_2-TPR tests.

Test	H_2 consumed by Co_3O_4 in **Co** (mmol/$g_{cat.}$)	H_2 consumed by CeO_2 surface O_x^{n-} in **Co@Ce** (μmol/$g_{cat.}$)	H_2 consumed by CeO_2 surface O_x^{n-} in **Ag/Co@Ce** (μmol/$g_{cat.}$)	H_2 consumed by Co_3O_4 in **Ag/Co@Ce** (mmol/$g_{cat.}$)
H_2-TPR	11.4	224.0	290.4	7.6
O_2-1 st	11.5	199.3	280.0	7.2
O_2-2nd	9.9	196.2	510.8	7.2

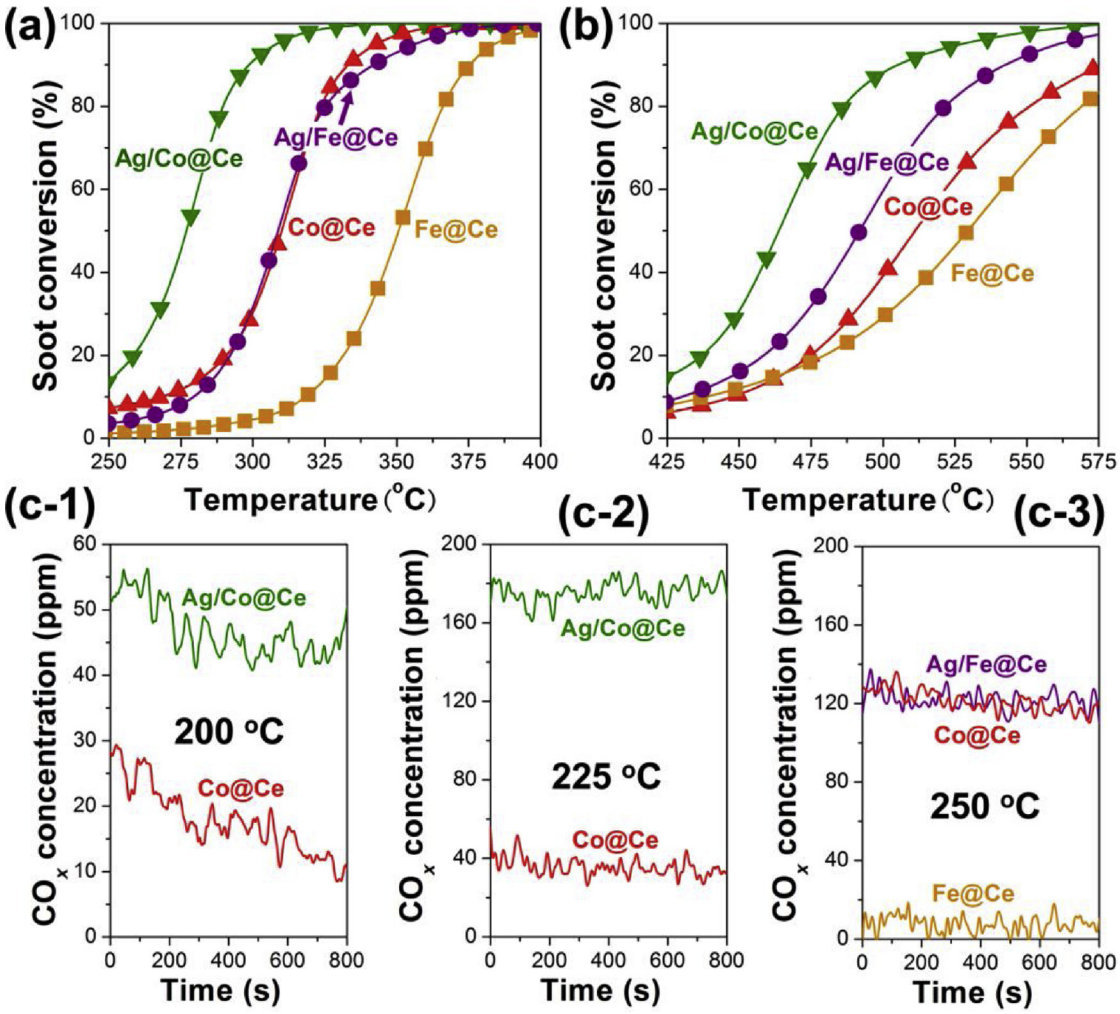

Fig. 6. Soot conversion during soot-TPO tests under the (a) "tight" and (b) "loose" contact mode and CO_x production during isothermal soot oxidation under the "tight" contact mode. Reaction conditions: atmosphere = 1% O_2/N_2, catalyst/soot = 10/1, TPO heating rate = 5 °C/min.

Table 3
The activities of the catalysts during TPO reactions.

Catalyst	T_{50} in soot-TPO in 1% O_2/N_2, "tight" mode (°C)	T_{50} in soot-TPO in 1% O_2/N_2, "loose" mode (°C)	T_{50} in soot-TPO in 500 ppm NO/5% O_2/N_2, "loose" mode (°C)	T_{10} in NO-TPO (°C)
Co@Ce	310	511	419	192
Ag/Co@Ce	277	462	395	171
Fe@Ce	351	530	449	273
Ag/Fe@Ce	308	492	444	290

constant low NO_2 production (Ag/Co@Ce > Co@Ce > Co) instead of being inert. These results indicated two facts: (1) the lattice oxygen in Co_3O_4 and/or CeO_2 could maintain only a low NO → NO_2 conversion, (2) the shadowed area in Fig. 7c should be caused by O_2-derived unstable active species but not lattice oxygen. Given the surface O_x^- was an important reactivity descriptor for NO oxidation [13], whose concentration followed the sequence of Ag/Co@Ce > Co@Ce > > Co (Figs. 4 and 5), it was likely that the residual O_x- on CeO_2 contributed to NO_2 formation and retarded the activity loss of Ag/Co@Ce and Co@Ce.

3.7. Evaluation of catalysts' practical potential

The above results evidenced the high soot combustion activity of Ag/Co@Ce, whose potential application was further evaluated in the presence of water vapor—a common component in vehicle exhausts [2]. As shown in Fig. 8a and Figure S2, soot ignition was facilitated over both the silver-containing catalysts by introducing water, which could be attributed to the oxidation of soot by the additional hydroxyl species [13]. Specifically, for Ag/Co@Ce with high NO_2 production (Fig. 7b), the formation of HNO_3 ($3NO_2 + H_2O \rightarrow 2HNO_3 + NO$) and its catalytic performance caused a significant T_{50} decrease (395 °C → 370 °C) [4]. Such a high activity of Ag/Co@Ce overwhelmed that of platinum. Actually, even after a hydrothermal ageing in 10% H_2O/air at 800 °C for 10 h, Ag/Co@Ce still oxidized soot easier than 1% Pt/Al_2O_3 (pre-reduced) did (Fig. 8b). Since platinum was among the most active commercial catalysts for NO and soot oxidation [2–4], the practical potential of Ag/Co@Ce was considerably high.

Besides being active and stable, practical catalysts should also be easily fabricated. Gratifyingly, it was observed that a simple precipitation method led to formation of the CeO_2-on-Co_3O_4 morphology. As shown in Fig. 9a-1, a-2 and Figure S3, similar to the results obtained by Guo et al. [45], the co-precipitated CoCe catalyst (Co:Ce = 5:1) was consisted of CeO_2 grains scattering on large Co_3O_4 particles. There were also a few isolated CeO_2 aggregations (Fig. 9a-3 and a-4). In this sense, CoCe could be regarded as the degraded version of Co@Ce which contained incomplete Co_3O_4@CeO_2 core-shell structure.

As shown in Fig. 9b and Figure S4, with low concentration of O_2 (1%) as the only oxidant, Ag/CoCe and CoCe combusted 50% soot at temperatures 20 °C and 23 °C higher than those of Ag/Co@Ce and

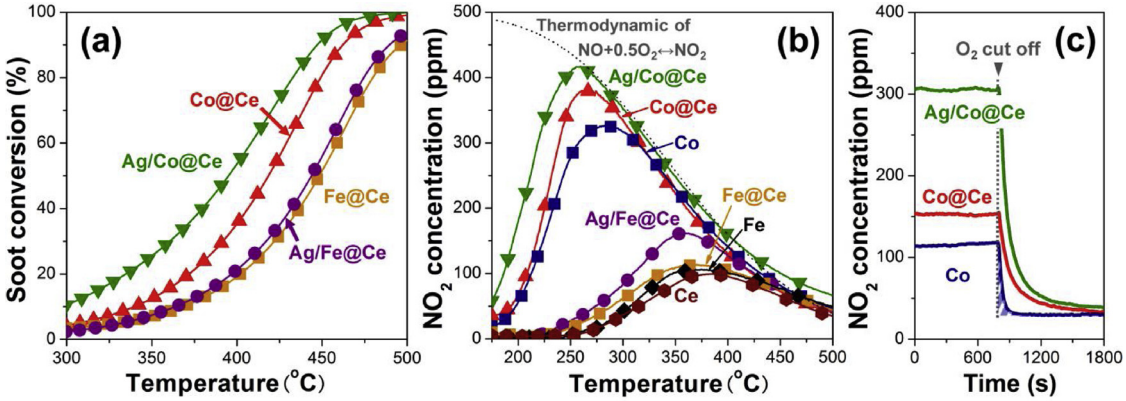

Fig. 7. (a) Soot conversion during soot-TPO tests under the "loose" contact mode, NO_2 production during (b) NO-TPO and (c) isothermal NO oxidation at 220 °C. Reaction conditions: atmosphere = 500 ppm NO/5% O_2/N_2, catalyst/soot in soot-TPO = 10/1, TPO heating rate = 5 °C/min.

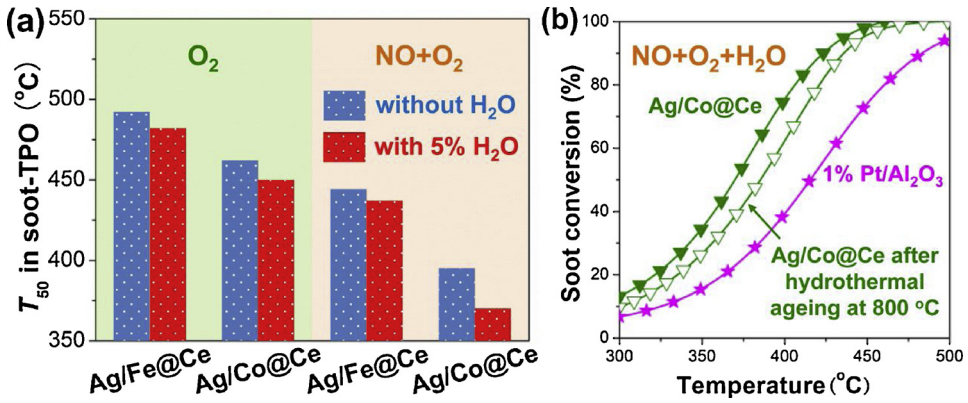

Fig. 8. Soot oxidation behavior of the catalysts under (a) 1% O_2/N_2 or 500 ppm NO/5% O_2/N_2, with or without 5% H_2O and (b) 500 ppm NO/5% O_2/5% H_2O/N_2. Reaction conditions: catalyst/soot = 10/1 ("loose" contact mode), TPO heating rate = 5 °C/min.

Co@Ce, respectively. The activity gaps between core-shell catalysts and their componential copies became smaller when NO_x was involved. These results indicated that the combustion of soot in O_2/N_2 was affected strongly by the oxygen supply from Co_3O_4, which could be accelerated remarkably with integrated CeO_2 and Ag/CeO_2 coating [14]. In contrast, the "NO_2-assisted" soot combustion relied heavily on NO → NO_2 conversion [4,19], in which Co_3O_4 itself played a crucial role [25–28]. Therefore, it was not surprising that catalysts with similar cobalt contents oxidized the loosely contacted soot similarly with NO_x. In any case, the easily-fabricated Ag/CoCe and CoCe ignited soot at lower temperatures than the highly active Pt/Al_2O_3, suggesting the superior practicability of the Co_3O_4-driven catalytic system in this study.

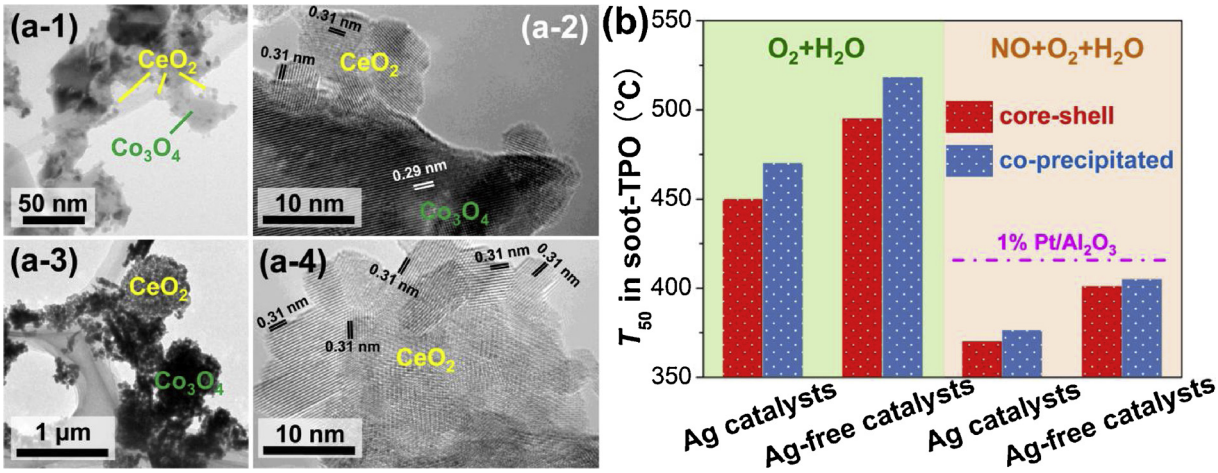

Fig. 9. (a) TEM images of CoCe, (b) oxidation behavior of the Co_3O_4-CeO_2-based catalysts under 1% O_2/5% H_2O/N_2 or 500 ppm NO/5% O_2/5% H_2O/N_2. Reaction conditions: catalyst/soot = 10/1 ("loose" contact mode), TPO heating rate = 5 °C/min.

4. Discussion

4.1. Soot oxidation in O_2

As is well known, soot was oxidized by ceria via a Mars-van Krevelen-like mechanism. During reactions in presence of O_2, the active species—O_x^- on CeO_2 surface—was repeatedly consumed by soot and regenerated by lattice and gaseous oxygen [9–14]. Although the oxygen vacancies (Ce^{3+}-V_O) played important roles in converting O_2 into O_x^- (Ce^{3+}-V_O + 0.5xO_2 → Ce^{4+}-O_x^-), their presence and dynamic change brought about uncertainty in catalysts' performance [53]. Moreover, the insufficient supply of gaseous O_2 in GPF made the O_2 → O_x^- regeneration route unreliable [54]. Therefore, deep utilization of catalyst lattice (bulk) oxygen could be an alternative way out. Based on this assumption, core-shell catalysts with oxides (e.g. Co_3O_4 and Fe_2O_3) coated by Ag/CeO_2 were designed, which could transfer bulk oxygen of catalyst onto soot efficiently through a tandem delivery route (i.e. MO_x → CeO_2 → Ag) [14]. Specifically, the Ag/Co@Ce catalyst studied in this work was extremely active for soot oxidation in O_2, whose superiority came mainly from three aspects.

First, as the inner core and the main component of Ag/Co@Ce, Co_3O_4 nanocubes contained a large amount of readily reducible lattice oxygen. As evidenced by H_2-TPR, Co_3O_4 itself contributed much more oxygen at 100~350 °C than any other samples (Fig. 4b). This could be attributed to its low metal-oxygen bond energy and broad range of the bulk non-stoichiometry [22,23,55]. More importantly, in comparison with Fe_2O_3, the smaller effective activation energy and lower Tammann temperature of Co_3O_4 conferred higher mobility to its surface/subsurface lattice oxygen [20,55]. As a result, Co_3O_4 was able to deliver its lattice oxygen to reductants (e.g. H_2 or soot) at much lower temperatures than Fe_2O_3 did (Figure S5).

Second, CeO_2 coating amplified the utilization of oxygen in Co_3O_4. Due to the narrow non-stoichiometry range of CeO_2, it was less reducible than Co_3O_4 [28,29]. However, the easy Ce^{3+} ↔ Ce^{4+} shuffling conferred CeO_2 high oxygen release/storage speed, making CeO_2 qualified as an "oxygen gateway" to pump out the bulk oxygen of Co_3O_4 [56]. The higher reduction potential of Co^{3+}/Co^{2+} (1.92 V) than Ce^{4+}/Ce^{3+} (1.62 V) also facilitated this oxygen transfer. Consequently, a large amount of Co_3O_4 bulk oxygen migrated to CeO_2, resulting in the abundant ceria lattice oxygen of Co@Ce (Ce^{3+}/Ce^{4+} = 0.27, Table 1). By utilizing these lattice oxygen species, Co@Ce produced plentiful O_x^- (Ce^{4+}-O^{2-} ↔ O^- ↔ O_2^-) either with (Fig. 5b) or without (Fig. 4c) the assistance of gaseous O_2 [7,8]. These O_x^- ignited the soot particles on CeO_2 surface easily [9], resulting in the lower soot combustion temperature of Co@Ce in comparison with Co (Fig. 6).

It is worth noting that, the core-shell structure conferred Co@Ce not only high initial activity but also good stability. As shown in Fig. 3b, Co@Ce exhibited slightly higher Co^{2+} content after reacting with soot at 225 °C, indicating its inner oxygen delivery (Co_3O_4 → CeO_2). Thanks to this continuous bulk oxygen supply, the Ce^{3+} content in CeO_2 was almost intact after the reactions (Figure S6). These results demonstrated that, Co@Ce avoided the continuous generation of the soot-derived Ce^{3+}-V_O to a large extent [53]. Therefore, instead of being affected by the V_O-induced O_2^- → O^- → O^{2-} transformation [11], Co@Ce regenerated O_x^- stably in redox cycles. This was in accordance with the cycled TPR results (Fig. 5b), which explained the high stability of Co@Ce during the isothermal reaction at 225 °C (Fig. 6c-2).

Finally, the Ag nano-particles on CeO_2 surface completed the "tandem oxygen delivery route" of Ag/Co@Ce. According to the generalized Cabrera–Mott theory, silver with low work function could "pump out" the lattice oxygen of ceria via back spillover effect [13,50]. When soot was oxidized on catalyst surface, the oxygen gradient actuated the tandem oxygen delivery (Co_3O_4 → CeO_2 → Ag) that provided lattice oxygen continuously. Moreover, gaseous O_2 could be adsorbed and activated by silver, resulting in the formation of O_x^- (Ag + O_2 → Ag^+ + O_2^-) [51]. Consequently, Ag/Co@Ce exhibited far better O_x^- generation (Fig. 4c) and regeneration (Fig. 5c and Table 2) ability in comparison with Co@Ce. This explained why Ag/Co@Ce was both reactive and stable at a temperature as low as 200 °C (Fig. 6c), which led to further decreased soot ignition temperature in the soot-TPO tests (Table 3).

4.2. Soot oxidation in NO + O_2

When NO_x was involved in the reaction, NO_2 became the leading soot igniter [19]. As shown in Figure S7, for the cobalt-based catalysts, the "O_2-assisted" soot oxidation route was totally overwhelmed by the "NO_2-assisted" one at low temperatures. The benefit of NO_2 could be further amplified with the assistance of H_2O (Fig. 8). Therefore, in order to reveal the mechanism behind Ag/Co@Ce's superior soot oxidation activity in presence of NO_x, close attention should be paid to its NO → NO_2 conversion behavior.

As indicated by Weiss et al., due to the high electrochemical redox potential of Co^{3+}/Co^{2+}, Co_3O_4 could activate O_2 easily and thereby was a robust NO oxidizer. They also highlighted the faster NO oxidation turnover on larger Co_3O_4 clusters, which was attributed to their easier O_2 activation [25]. In this sense, a high dispersion of Co_3O_4 (e.g. < 10 nm in size) was not indispensable for achieving satisfying NO conversion. This agreed with the high NO oxidation activity of the 20–40 nm Co_3O_4 grains [57]. Therefore, it was not surprising that the cube-like Co_3O_4 inner cores (36 nm) provided Co@Ce and Ag/Co@Ce high basic NO_2 production rates (Fig. 7b). Interestingly, after coating Co_3O_4 with weaker NO oxidizers like CeO_2 and silver [39], its NO_2 production was amplified (Fig. 7b). This could be explained from two aspects.

On one hand, the O_x^- species provided by the Ag/CeO_2 shell promoted low-temperature NO oxidation. NO was oxidized by ceria through a nitrate-meditated Mars-van Krevelen mechanism reportedly, which could be accelerated by the participation of active oxygen ($O^{\#}$ = O_x^-) [13]:

$$NO + Ce^{3+} - O^{\#} \rightarrow Ce^{4+}\text{-}NO_2^- \quad (1)$$

$$Ce^{4+}\text{-}NO_2^- + O^{\#} \rightarrow Ce^{4+}\text{-}NO_3^- \quad (2)$$

$$Ce^{4+}\text{-}NO_3^- \rightarrow Ce^{3+} - O^{\#} + NO_2 \quad (3)$$

Thanks to the large amounts of O_x^- on Co@Ce and Ag/Co@Ce in comparison with Co (Fig. 5), the above O_x^--assisted route facilitated the NO_2 production over the ceria-coated samples. Importantly, even when gaseous O_2 was cut off, O_x^- might still get replenished from ceria lattice oxygen (e.g. form the Co_3O_4 → CeO_2 inner oxygen delivery) [11–14]. Similar to the results obtained by Zhang et al. [58], these O_x^- species reacted with NO and retarded the activity loss of Co@Ce and especially Ag/Co@Ce in the anaerobic reaction (Fig. 7c). It is worth noting that, the contribution of O_x^- to NO → NO_2 conversion outstood only at low temperatures. As shown in Fig. 10, the superiority of the O_x^--rich Ag/Co@Ce peaked at around 200 °C and then decreased as the temperature increased further. This indicated that at higher temperatures (e.g. > 225 °C), the Co_3O_4 inner cores themselves were activated and involved essentially in the reactions, making the role of O_x^- relatively less important.

On the other hand, the synergy between Co_3O_4 and CeO_2 facilitated the oxidation of NO at mild and high temperatures. The nanocubic Co_3O_4 inner cores were the main active phase herein, which were far more active than CeO_2 and silver for NO oxidation (Fig. 7b). Different from CeO_2, NO was reportedly oxidized by CoO_x through an ER surface process, involving kinetically relevant O_2 binding at unoccupied sites (*) on the cluster surfaces that were almost saturated with chemisorbed oxygen atoms (O*) [25,59,60]:

$$O_2 + 2^* \rightarrow 2O^* \quad (4)$$

$$NO + O^* \rightarrow NO_2 + * \quad (5)$$

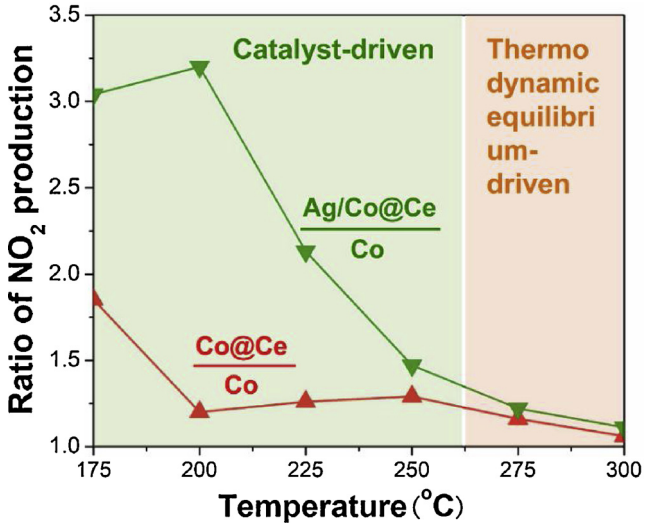

Fig. 10. Ratios of NO_2 production over the catalysts as a function of temperature during the NO-TPO tests in Fig. 7b.

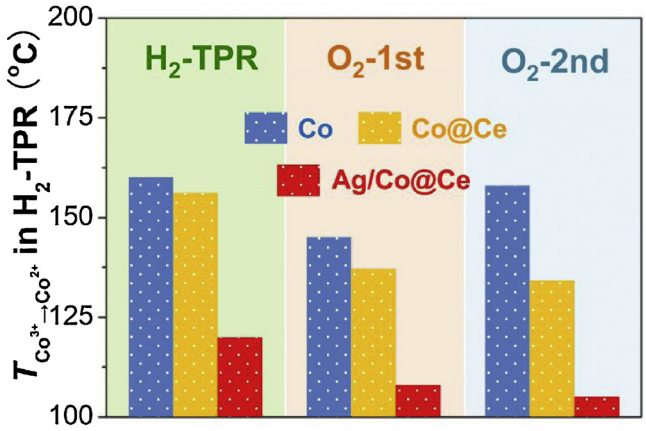

Fig. 11. Temperature of Co_3O_4 initial reduction in the catalysts during the TPR tests derived from Fig. 5.

Such a difference in reaction mechanisms was supported by the low participation of Co_3O_4 lattice oxygen-derived active species in the anaerobic reaction (Fig. 7c). For reaction (4), the availability of the one-electron oxidation–reduction cycle ($Co^{3+} \rightarrow Co^{2+}$) was crucial [25], which was also responsible for the Co^{2+} increase of Co@Ce after isothermal NO oxidation (Fig. 3b). As shown in Fig. 11, H_2 reduced Co_3O_4 more easily over Co@Ce and Ag/Co@Ce than over Co, especially during the cycled reactions (the O_2-1st and O_2-2nd results). Given the first step of Co_3O_4 reduction was $Co^{3+} \rightarrow Co^{2+}$ [31,32], it was reasonable to suggest that the CeO_2 and Ag/CeO_2 coating facilitated the $Co^{3+} \rightarrow Co^{2+}$ transformation during NO oxidation reactions. Similar promotion effect was reported previously by Bera et al., who indicated that Cu species in a Cu/CeO_2 matrix required less energy to be reduced and oxidized than in the case of pure CuO [47]. In this sense, with accelerated turnover of NO oxidation on Co_3O_4, Co@Ce and Ag/Co@Ce exhibited higher NO_2 production and thereby easier (NO_2-assisted) soot combustion than Co did.

5. Conclusions

In this study, by building core-shell tandem oxygen delivery ($MO_x \rightarrow CeO_2 \rightarrow Ag$) systems with nanocubic Co_3O_4 as the inner cores, robust $Ag/Co_3O_4@CeO_2$ catalysts with superior soot combustion activity were obtained. Based on the exploration of catalysts' structure and catalytic behavior in different conditions, several conclusions can be drawn as:

(1) Due to the easy oxygen release and high NO oxidation activity of Co_3O_4, it was a more effective component for soot oxidation catalysts in comparison with Fe_2O_3.
(2) With O_2 as the main oxidant, the O_x^- species generated by tandem oxygen delivery ($Co_3O_4 \rightarrow CeO_2 \rightarrow Ag$) dominated the catalytic oxidation of soot.
(3) With NO_x involving in the reactions, the CeO_2 and Ag/CeO_2 coatings boosted both the production of O_x^- and the NO conversion over Co_3O_4, resulting in soot ignition at relatively low temperatures via the "NO_2-assisted" route.

What is more important, the $Ag/Co_3O_4@CeO_2$ catalysts with high cost-efficiency and hydrothermal stability could be fabricated via a simple co-precipitation method with only minor activity degradation. This indicated that the ternary system was highly practical for application in catalyzed gasoline and diesel particulate filters (CGPFs and CDPFs).

Acknowledgements

The authors would like to acknowledge the National Key R&D Program of China (Project 2017YFC0211202), the National Natural Science Foundation of China (Grant No. 51702304), the Natural Science Foundation of Shandong Province (Grant No. ZR2017BEM006), the Young Elite Scientists Sponsorship Program by CAST (2018QNRC001), the Postdoctoral Science Foundation of Shandong Province (Grant No. 201601009), Qingdao City Programs for Science and Technology Plan Projects (18-2-2-2-jch) and the Fundamental Research Funds for the Central Universities (201861050).

Appendix A. Supplementary data

Supplementary material related to this article can be found, in the online version, at doi:https://doi.org/10.1016/j.apcatb.2019.03.019.

References

[1] T. Johnson, SAE Technical Series Paper 2014-01-1491, (2014).
[2] B.A.A.L. van Setten, M. Makkee, J.A. Moulijn, Catal. Rev. 43 (2001) 489–564.
[3] D. Fino, V. Specchia, Powder Technol. 180 (2008) 64–73.
[4] S. Liu, X. Wu, H. Luo, D. Weng, R. Ran, J. Phys. Chem. C 119 (2015) 17218–17227.
[5] J.M. Richter, R. Klingmann, S. Spiess, K. Wong, SAE Technical Series Paper 2012-01-1244, (2012).
[6] S. Liu, X. Wu, D. Weng, R. Ran, J. Rare Earth. 33 (2015) 567–590.
[7] J. Haber, B.K. Warren, S.T. Oyama (Eds.), Heterogeneous Hydrocarbon Oxidation, vol. 638, ACS Symp. Series, 1996, p. 20.
[8] J. Haber, Fundamentals of Hydrocarbon Oxidation, Handbook of Heterogeneous Catalysis: Online, (2008), p. 3359.
[9] M. Machida, Y. Murata, K. Kishikawa, D. Zhang, K. Ikeue, Chem. Mater. 20 (2008) 4489–4494.
[10] K. Shimizu, H. Kawachi, A. Satsuma, Appl. Catal. B 96 (2010) 169–175.
[11] S. Liu, X. Wu, W. Liu, W. Chen, R. Ran, M. Li, D. Weng, J. Catal. 337 (2016) 188–198.
[12] Y. Gao, A. Duan, S. Liu, X. Wu, W. Liu, M. Li, S. Chen, X. Wang, D. Weng, Appl. Catal. B 203 (2017) 116–126.
[13] H. Wang, S. Luo, M. Zhang, W. Liu, X. Wu, S. Liu, J. Catal. 368 (2018) 365–378.
[14] H. Wang, B. Jin, H. Wang, N. Ma, W. Liu, D. Weng, X. Wu, S. Liu, Appl. Catal. B 237 (2018) 251–262.
[15] J.C. Martínez-Munuera, M. Zoccoli, J. Giménez-Mañogil, A. García-García, Appl. Catal. B 245 (2019) 706–720.
[16] D. Rathod, M. Hoffman, S. Onori, Z. Filipi, Experimental investigation of soot accumulation and regeneration in a catalyzed gasoline particulate filter utilizing particulate quantification and gas speciation measurements, ASME International Combustion Engine Fall Technical Conference (2019).
[17] X. Mou, B. Zhang, Y. Li, L. Yao, X. Wei, D. Su, W. Shen, Angew. Chem. Int. Ed. 51 (2012) 2989–2993.
[18] D. Reichert, T. Finke, N. Atanassova, H. Bockhorn, S. Kureti, Appl. Catal. B 84 (2008) 803–812.
[19] A. Bueno-López, Appl. Catal. B 146 (2014) 1–11.
[20] G. Jian, L. Zhou, N.W. Piekiel, M.R. Zachariah, ChemPhysChem 15 (2014) 1666–1672.
[21] J.M. Christensen, J. Grunwaldt, A.D. Jensen, Appl. Catal. B 188 (2016) 235–244.

[22] Y. Yu, T. Takei, H. Ohashi, H. He, X. Zhang, M. Haruta, J. Catal. 267 (2009) 121–128.
[23] V.A. Sadykov, L.A. Isupova, I.A. Zolotarskii, L.N. Bobrova, A.S. Noskov, V.N. Parmon, E.A. Brushtein, T.V. Telyatnikova, V.I. Chernyshev, V.V. Lunin, Appl. Catal. A Gen. 204 (2000) 59–87.
[24] L. Hu, Q. Peng, Y. Li, J. Am. Chem. Soc. 130 (2008) 16136–16137.
[25] B.M. Weiss, N. Artioli, E. Lglesia, ChemCatChem 4 (2012) 1397–1404.
[26] M.M. Yung, E.M. Holmgreen, U.S. Ozkan, J. Catal. 247 (2007) 356–367.
[27] M.F. Irfan, J.H. Goo, S.D. Kim, Appl. Catal. B 78 (2008) 267–274.
[28] J. Xu, G. Lu, Y. Guo, Y. Guo, X. Gong, Appl. Catal. A Gen. 535 (2017) 1–8.
[29] G. Zou, Y. Xu, S. Wang, M. Chen, W. Shang, Catal. Sci. Technol. 5 (2015) 1084–1092.
[30] G. Zou, Z. Fan, X. Yao, Y. Zhang, Z. Zhang, M. Chen, W. Shang, Chin. J. Catal. 38 (2017) 564–573.
[31] G. Zhai, J. Wang, Z. Chen, W. An, Y. Men, Chem. Eng. J. 337 (2018) 488–498.
[32] M. Khasu, T. Nyathi, D.J. Morgan, G.J. Hutchings, M. Claeys, N. Fischer, Catal. Sci. Technol. 7 (2017) 4806–4817.
[33] Y. Teng, Y. Kusano, M. Azuma, M. Haruta, Y. Shimakawa, Catal. Sci. Technol. 1 (2011) 920–922.
[34] E.E. Miró, F. Ravelli, M.A. Ulla, L.M. Cornaglia, C.A. Querini, Catal. Today 53 (1999) 631–638.
[35] P.G. Harrison, I.K. Ball, W. Daniell, P. Lukinskas, M. Céspedes, E.E. Miró, M.A. Ulla, Chem. Eng. J. 95 (2003) 47–55.
[36] S.K. Megarajan, S. Rayalu, Y. Teraoka, N. Labhsetwar, J. Mol. Catal. A Chem. 385 (2014) 112–118.
[37] M.Á. Stegmayer, V.G. Milt, N. Navascues, E. Gamez, S. Irusta, E.E. Miró, Mol. Catal. (2018), https://doi.org/10.1016/j.mcat.2018.07.011.
[38] J. Liu, Z. Zhao, J. Wang, C. Xu, A. Duan, G. Jiang, Q. Yang, Appl. Catal. B 84 (2008) 185–195.
[39] H. Wang, S. Luo, X. Li, W. Liu, X. Wu, D. Weng, S. Liu, Catal. Today (2018), https://doi.org/10.1016/j.cattod.2018.06.027.
[40] A. Serve, A. Boréave, B. Cartoixa, K. Pajot, P. Vernoux, Appl. Catal. B 242 (2019) 140–149.
[41] W.Y. Hernández, D. Lopez-Gonzalez, S. Ntais, C. Zhao, A. Boréave, P. Vernoux, Appl. Catal. B 226 (2018) 202–212.
[42] W. Yang, S. Wang, K. Li, S. Liu, L. Gan, Y. Peng, J. Li, Chem. Eng. J. 364 (2019) 448–451.
[43] M. Machida, T. Kawada, H. Fujii, S. Hinokuma, J. Phys. Chem. C 119 (2015) 24932–24941.
[44] M.C. Biesinger, B.P. Payne, A.P. Grosvenor, L.W.M. Lau, A.R. Gerson, R.S.C. Smart, Appl. Surf. Sci. 257 (2011) 2717–2730.
[45] Q. Guo, Y. Liu, Appl. Catal. B 82 (2008) 19–26.
[46] D.M. Gómez, V.V. Galvita, J.M. Gatica, H. Vidal, G.B. Marin, Phys. Chem. Chem. Phys. 16 (2014) 11447–11455.
[47] P. Bera, S. Mitra, S. Sampath, M.S. Hegde, Chem. Commun. (2001) 927–928.
[48] I.I. Soykal, H. Sohn, J.T. Miller, U.S. Ozkan, Top. Catal. 57 (2014) 785–795.
[49] V.V. Pushkarev, V.I. Kovalchuk, J.L. d'Itri, J. Phys. Chem. B 108 (2004) 5341–5348.
[50] Q. Fu, T. Wagner, Surf. Sci. Rep. 62 (2007) 431–498.
[51] M. Schmidt, A. Masson, C. Bréchignac, Phys. Rev. Lett. 91 (2003) 243401.
[52] A. Setiabudi, M. Makkee, J.A. Moulijn, Appl. Catal. B 50 (2004) 185–194.
[53] H. Wang, S. Liu, Z. Zhao, X. Zou, M. Liu, W. Liu, X. Wu, D. Weng, Catal. Sci. Technol. 7 (2017) 2129–2139.
[54] E. Aneggi, Cd. Leitenburg, A. Trovarelli, Catal. Today 181 (2012) 108–115.
[55] C. Doornkamp, M. Clement, V. Ponec, J. Catal. 182 (1999) 390–399.
[56] M. Machida, T. Kawada, H. Fujii, S. Hinokuma, J. Phys. Chem. C 119 (2015) 24932–24941.
[57] Z. Ren, Y. Guo, Z. Zhang, C. Liu, P. Gao, J. Mater. Chem. A 1 (2013) 9897–9906.
[58] Z. Zhang, D. Han, S. Wei, Y. Zhang, J. Catal. 276 (2010) 16–23.
[59] R. Aslam, M.R. Usman, M.F. Irfan, J. Environ. Chem. Eng. 4 (2016) 2871–2877.
[60] M.W. Penninger, C.H. Kim, L.T. Thompson, W.F. Schneider, J. Phys. Chem. C 119 (2015) 20488–20494.